

SHORT-WAVE INSTABILITY GROWTH IN CLOSELY SPACED VORTEX PAIRS

Nicholas BOUSTEAD^{*}, Kris RYAN and Gregory J SHEARD

¹ Department of Mechanical Engineering, Monash University, Victoria 3800, AUSTRALIA

^{*}Corresponding author, E-mail address: Nichoas.Boustead@eng.monash.edu.au

ABSTRACT

The dissipation of vortex pairs is an important field of study for the aviation industry in which enhanced vortex dissipation may lead to increased efficiency of aircraft infrastructure. The growth of short-wave elliptical instabilities in a Lamb-Oseen vortex pair subject to non-uniform strain fields at close vortex spacing is considered using direct numerical simulation techniques at a Reynolds number $Re=20000$. Much research has previously been conducted at relatively large vortex spacing where the mutually induced strain field causing the elliptical deformation of vortex cores is typically uniform. This study investigates the instability growth over a range of wave-numbers and analyses the change in growth as the vortex spacing is reduced. This is completed using linear stability analysis. The study demonstrates that as vortex spacing is reduced, the growth rate of all instability mode frequencies is enhanced relative to that of the fastest growing mode. A coupling of vortices is observed at close vortex spacing, which may lead to improved non-linear instability growth, and the development of fluid cross-over regions. These fluid cross over regions are shown to be products of a linear growth regime. They exist at large separations but are greatly enhanced at close separation distances.

NOMENCLATURE

a	vortex core radius	Ω	domain
b	vortex separation	k	wave-number
a/b	size / separation ratio	λ	wavelength
Γ	circulation	t_1	evolution time
t^*	normalized settling time	n	profile steepness
ω_z	axial vorticity component	T	time of growth
σ	instability growth rate	L_2	L2 Norm
μ	stability multiplier	ν	viscosity
Re	Reynolds number		

INTRODUCTION

The study of vortex dynamics is important to the mineral processes industry in relation to cyclonic separation. It is also pivotal to the aviation industry in which the generation of large-scale, coherent vortices at the wingtips of large aircraft can present a significant hazard to aircraft downstream, where air flows are not uniform (Spalart, P. 1998). Thus a minimum safe distance between aircraft launches must be maintained.

A pair of counter-rotating vortex pairs is created at the wing tips of aircraft as a product of the lift produced on the wings (Phillips 2004). Studies of these vortices have generally considered vortices with a Lamb-Oseen profile

(figure 1), which is a counter-rotating pair with Gaussian vorticity profile. The vorticity profile of the Lamb-Oseen Vortex pair may be expressed mathematically by

$$\omega_z = \frac{\Gamma}{\pi a_0^2} e^{-r^2/a_0^2}, \quad (1)$$

where ω_z is the axial vorticity component, a is the characteristic core radius of the vortex (a_0 is the core radius at time $t = 0$), and Γ is the circulation.

Over time aircraft wakes develop the Gaussian profile of the Lamb-Oseen vortex pair, with an additional velocity component in-line with the axis of the vortex. Many factors may contribute to the strength of the Lamb-Oseen pair, including aircraft size, speed, weight and lift coefficient (Phillips 2004). In their investigation of co-rotating vortices, Le Dizes and Verga (2002) show that diffusion relaxes any non-Gaussian axis-symmetrical vortex towards that of a Gaussian profile. Thus the Gaussian profile of a Lamb-Oseen vortex pair offers a reasonable approximation to wing-tip vortices.

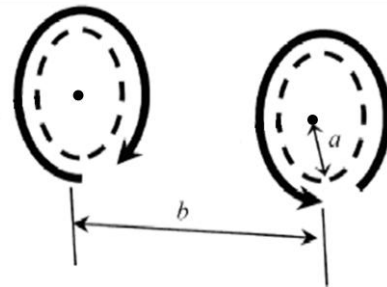


Figure 1: Schematic representation of flow in a counter-rotating Lamb-Oseen pair with a Gaussian profile. a is the characteristic core radius, b is the separation distance.

Le Dizes and Laporte (2002) described the capacity of paired vortices to exert reciprocal strain fields that elliptically deform each vortex core. Le Dizes and Verga (2002) identified three key parameters contributing to the elliptical deformation process: vortex steepness n , Reynolds number and separation ratio (a/b). Vortex steepness is described by,

$$\omega_0(r) = \exp(-r^{2n}) \quad (2)$$

where n is the vortex steepness and $n=1$ gives a Gaussian vortex, and ω_0 is the vorticity. Reynolds number is defined as,

$$Re = \Gamma/\nu \quad (3)$$

where Γ is the circulation and ν is the viscosity.

Elliptical deformations are driven by the mutually induced strain field of the vortex core. At large separations the strain field near the partner vortex core may be assumed

uniform, at closer separations however the strain field is curved.

Sipp *et al* (2000) also showed that the elliptical deformation proceeds regardless of the initial vorticity profile, relaxing the vortices to a unique Gaussian state which is independent of the Reynolds number. This validates the use of a Lamb-Oseen pair in examining elliptical instabilities.

Previous studies of vortex pair dissipation have identified factors that contribute to the growth rate of instabilities in vortex pairs. These include centrifugal instability, vortex merging, vortex straining, and the effect of viscous damping, (Le Dizès & Laporte 2002). The elliptical instability mechanism has been identified as the greatest dissipating force of Lamb-Oseen vortex pairs. This results from the resonant coupling of two vortex modes, with the strain field produced by the vortex pair (Le Dizès & Laporte 2002).

Instabilities may be classified as either long-wavelength Crow instabilities or short-wavelength elliptical instabilities shown in figure 2. In a numerical study, Le Dizès and Laporte (2002) observed the short-wave instabilities as in-phase oscillations of the vortex core.

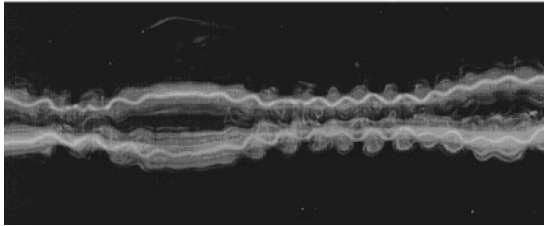


Figure 2: Visualization of vortices under combined long and short-wavelength instabilities. The sinusoidal wave-packet of the vortex axis is induced by Crow instabilities. The inner high frequency oscillation results from short-wave instabilities. Source: Leweke and Williamson (1998)

Leweke and Williamson (1998) concluded the elliptical instability of the two vortices evolves in a distinct phase relationship, breaking the initial symmetry of the pair. This they attribute to the coupling of instabilities, which produces an asymmetric mode to satisfy kinematic matching conditions. Leweke and Williamson's study also described the long-term evolution of the instability, demonstrating that the growing deformation of the short-wave instabilities gives rise to periodic cross-over of fluid between vortices. This creates an array of secondary vortices perpendicular to the primary pairs. The secondary vortices quickly lead to the breakdown of primary vortex circulation, as observed by Ryan and Sheard (2002). Leweke and Williamson proposed that the classical Crow instability is in fact the result of a long and short-wave instability interaction. They suggested that the long-wave instability causes vortex cores to exist closer in certain regions, leading to an increased growth rate of short-wave instabilities and hence secondary vortex formation in these regions.

The array of secondary vortices identified by Leweke and Williamson (1998) evolve in the non-linear growth phase of the (-1, 1) Kelvin mode. Ryan and Sheard (2007) demonstrated that the (-1, 1) Kelvin mode has the greatest dissipation rate for flows of this type as a result of production of secondary vortices. This is due to a non-linear growth zone of short-wave instabilities. A large

growth rate during the linear phase proved insufficient to produce enhanced vortex dissipation in a Kelvin type mode. (Kelvin modes are a classification scheme for the eccentricity and ellipticity of instability modes). The numerical study employed may not have accounted for viscous diffusion, which moves the vortices closer together over time. This in turn may assist in the production of secondary vortices.

Review of pertinent literature indicates that these relationships are only consistent when vortices are sufficiently separated so as to feel only a uniform strain field. Little is known about the propagation of short-wave instability modes at small vortex spacing (Le Dizès & Laporte 2002). As such this investigation aims to analyse the effects of short-wave instability modes at small vortex spacing. Previous work has been limited to a maximum vortex separation ratio $a/b=0.25$. This will be the lower limit of the determining parameter on the elliptical core deformation. The analysis is to be executed at a Reynolds number of 20,000.

Elliptical instabilities are formed in both co-rotating (Leweke & Meunier 2005) and counter-rotating vortex pairs (Leweke & Williamson 1998), however for the purpose of aeronautical applications this paper will concentrate only on the counter-rotating case, for which vortex merging does not occur.

METHODOLOGY

The stability of a closely spaced Lamb-Oseen vortex pair is studied. A series of base flows are created in which the vortices are placed successively closer to each other relative to their size. The flow structures being studied are shown in figure 3.

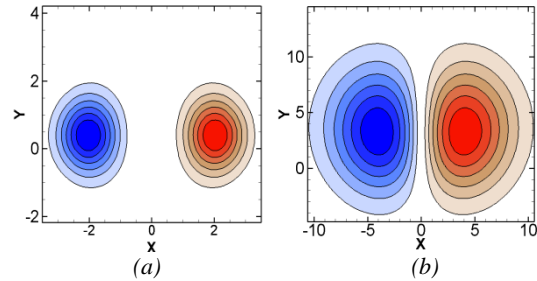


Figure 3: Vorticity profiles of vortex pairs a) is at $a/b=0.25$, b) is at $a/b=0.481$. Note the elliptical deformation in case b.

A spectral element technique is used to solve the incompressible Navier-Stokes equations

$$\frac{\partial \mathbf{u}}{\partial t} + (\mathbf{u} \cdot \nabla) \mathbf{u} = -\nabla P + \nu \nabla^2 \mathbf{u} \quad (4a)$$

$$\nabla \cdot \mathbf{u} = 0 \quad (4b)$$

where \mathbf{u} is the velocity vector, ∇ is the gradient operator, P is a scalar pressure and t is time.

The package uses an operator splitting technique (Karniadakis, Israeli & Orszag 1991), which allows the advection and diffusion terms to be solved independently for each time step. A spectral element method is used to discretise spatial terms. The domain is discretised into a series of macro elements within which, high-order tensor-product Lagrangian polynomials are employed as shape functions to solve the partial differential equations. A 3rd order accurate, backward multi-step method using a three-

step splitting scheme evolves the solution in time to solve the linearised time dependent Navier-Stokes equations.

During the perturbation study, a disturbance of single frequency is propagated in the vortex perpendicular to the 2D plane, acting along the axial direction of a vortex stream tube, allowing investigation of the susceptibility of the vortices to instabilities in the third dimension. To this end a global stability analysis is conducted in which the velocity and pressure fields (\mathbf{u}, p) are broken up in to a two dimensional base flow ($\bar{\mathbf{u}}, \bar{p}$) and a three dimensional disturbance (\mathbf{u}', p')

$$\mathbf{u} = \bar{\mathbf{u}} + \mathbf{u}', \quad p = \bar{p} + p' \quad (5a, b)$$

Substituting these into the Navier Stokes equations, cancelling the base flow terms and neglecting products of the (small) perturbation field yields,

$$\frac{\partial \mathbf{u}'}{\partial t} + (\bar{\mathbf{u}} \cdot \nabla) \mathbf{u}' + (\mathbf{u}' \cdot \nabla) \bar{\mathbf{u}} = -\nabla P' + \nu \nabla^2 \mathbf{u}' \quad (6)$$

The stability analysis is then carried out simply by integrating the perturbation field forward in time and monitoring the growth or decay of the field. The perturbation field evolves over one period subject to an operator \mathbf{A} as

$$\mathbf{u}'_{n+1} = \mathbf{A}(\mathbf{u}'_n) \quad (7)$$

The eigen-values of \mathbf{A} correspond to the Floquet multipliers of the system, μ ,

$$\mu = e^{\sigma T} \quad (8)$$

for which σ is the instability growth rate.

The two dimensional solver and stability analysis code has been used previously for a variety of flow problems for example Sheard, Leweke, Thompson & Hourigan (2007); Sheard, Fitzgerald & Ryan (2009)

SIMULATION OPTIMISATION

The mesh used in the vortex analysis consisted of an internal fine region and a coarser outer region which stretches to the edge of the domain where the boundary conditions were applied. When created, the vortices exist in the centre of the fine region. This is where the vorticity is most concentrated and accuracy is most important.

The two counter rotating vortices are created with a characteristic radius less than 2% of the computational domain width in all directions. Transient Dirichlet boundary conditions are added at the extents of the domain, which assesses the rate at which the vortices are advecting out of the central refined mesh region and apply a force which acts to keep the vortices fixed in space. This is done in order to accurately simulate the flow, ensuring no reflection off boundaries and maintaining the vortex position in the centre of the refined region of the mesh. The boundary is located over 100 vortex radii from the vortex pair which ensures the transient boundary conditions do not affect the underlying physics of the vortex interaction.

In order to optimise the accuracy of the grid a P-type grid resolution study was conducted; global and local noise parameters were measured in order to assess the grid's accuracy

To measure the global accuracy of the flow field, two parameters were measured. Integration over the domain provided an estimate of the vortex circulation, which may

be compared to the input value. The second parameter was the L_2 -norm, given by:

$$L_2 = \oint |u| d\Omega, \quad (9)$$

where $|u|$ is the magnitude of the velocity vector and Ω is the computational domain. The strain rate magnitude at the vortex core was used to assess the local noise in the solution.

These parameters were measured as the order of the polynomial used was changed. A 14th degree polynomial gave the most accurate solution with respect to both local and global noise. A Richardson extrapolation of both global noise measurements, using a power law fit estimated a maximum error of 3.8%.

BASE FLOW EVOLUTION

Le Dizes and Verga (2002), showed that vortices will grow larger in size over time, as a natural result of viscous diffusion. The initial separation distance of $a/b=0.25$ was formed at the conclusion of the grid resolution study. The amount the vortex core will diffuse is described by

$$a = \sqrt{a_0^2 + 4\nu t_1}, \quad (10)$$

where a_0 is the initial vortex characteristic radius, t_1 is the time taken to evolve this solution and ν is the viscosity. And

$$t^* = \frac{t_1 \Gamma}{2\pi a_0^2}, \quad (11)$$

where t^* is the normalised time defined by Le Dizes and Verga (2002), and Γ is the circulation. Le Dizes and Verga (2002) showed that a settling time of $t^*=40$ is sufficient for the vortices to adjust to the induced strain fields and form stable elliptical deformations.

Base flows of varying separation ratios were created using the viscous diffusion method employed by Le Dizes and Verga (2002). By lowering the Reynolds number to $Re=15\pi$ the influence of the viscous term in the Navier-Stokes equations is enhanced and the vortices are allowed to diffuse, increasing the characteristic radius a and thus increasing the separation ratio.

Figure 3 shows two different vortex spacings after viscous diffusion has been used to change the vortex core radius. At small vortex separations there is significant elliptical deformation of the core. Figure 4 shows the strain fields of the largest separation case considered, $a/b=0.481$. It can be clearly seen that the strain field is now curved close to each vortex core. It was a major assumption in analytical formulations such as those of Le Dizes and Laporte (2002) that vortices were sufficiently separated such that a uniform strain field could be assumed at the core.

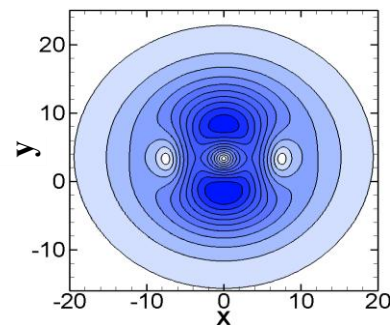


Figure 4: Stain field at vortex separation 0.481. Note the curved nature of the strain field at the cores

VORTEX SPACING LIMIT

During the evolution of the vortex base flows an upper limit for the separation ratio was discovered. The vortex spacing was accurately determined using a Simpson's 1/3rd quadrature method interpolating over the vortex region to find locations of maximum vorticity. The characteristic radius was determined using the axial vorticity ω_0 described by,

$$\omega_0 = \frac{\Gamma}{\pi a^2} \exp\left(-\left(\frac{r}{a}\right)^2\right) \quad (12)$$

It was found that as the vortices grew closer, the strain field of each vortex pushed on the neighbouring vortex forcing the pair further apart. Figure 5 shows that an upper limit of 0.5 for the vortex separation ratio. This implies that two vortices will never exist in the same space as defined by their characteristic core radii, i.e. their cores may never overlap. This also indicates that the strain field, while curved, will not permit periodic crossing of a shared vortex boundary. Given the majority of the vorticity is contained within the characteristic core radius; we would not physically expect counter-rotating vortices to be able to violate this boundary without destruction of the vortex structure.

Figure 5: Vortex separation ratio varying as radius a is diffused. Separation ratio converges toward 0.5.

PERTURBATION STUDY

A stability analysis was conducted on the vortex pair in which small disturbances were introduced of a specified axial wave-number. In this analysis the disturbance was evolved in a perturbation field, the effects of which may be observed by overlaying it over the frozen vortex base flow. Vortices of separation ratios $a/b=0.251$, 0.3625, 0.4063, 0.4257, 0.4385, and 0.447 were investigated. Each was subject to a series of disturbances in the normalised wavelength range of $\lambda/a=0.2$ to 5.0. Le Dizes and Laporte (2002) showed that this range is sufficient to describe the development of short-wavelength instabilities growing on a counter-rotating Lamb-Oseen vortex pair for small a/b . The following sections describe the instability growth in the vortex pair as the separation distance is changed.

INSTABILITY GROWTH RATE

The growth rate of the leading instability mode was monitored. For each case a disturbance was introduced characterised by its wave-number

$$k = 2\pi/\lambda, \quad (13)$$

where λ is the axial wavelength of the disturbance. The wave-number, k was changed such that results were taken at consistent values of normalised wavelength λ/a .

Figure 6 shows a comparison of the linear growth rate of elliptical instabilities as a function of the normalised axial wavelength, over different separation ratios a/b . The number of principal modes evident in each separation case varies as the non-uniform strain field acts to enhance or suppress instability modes. At a separation of $a/b=0.251$ three principal modes are evident. The first has a peak growth rate at $\lambda/a=1.15$, this peak was not reported by Le Dizes and Laporte (2002). The remaining peaks occur at $\lambda/a=1.6$ and at $\lambda/a=2.8$. The positions of this peak growth rate correlate with Le Dizes and Laporte's (2002) results for $a/b=0.18$ at $Re=\infty$, also shown in figure 6.

Figure 6: Growth rate of the elliptical instability as a function of the normalised axial wave-number. The dashed black line is Le Dizes and Laporte's results for $a/b=0.18$ case at $Re=\infty$. Legend describes a/b ratio.

The significant finding shown in figure 6 is that at closer vortex spacing the growth rate at all wavelengths is enhanced, relative to the peak growth rate. In addition we note the damping out of the $\lambda/a=1.15$ peak found in $a/b=0.251$. It is observed that in distantly separated cases the peak growth rates are sharp and well defined. As the vortices are brought closer together however, each peak broadens.

Critical wave-lengths where a local peak in growth rate is observed decrease as the distance between vortices decreases. The strongest mode is at $\lambda/a=2.8$ at a separation distance of $a/b=0.251$ but decreases to $\lambda/a=1.8$ at $a/b=0.447$, this is observed as a lateral shifting of the peak structures in figure 6. Furthermore the growth rates of the instabilities vary with vortex separation. Figure 7 shows the normalised growth rate of the peak instability mode in each separation case. It can be seen that after an initial increase in growth rate, the growth rate of the peak instability mode decreases as the vortices are brought closer together

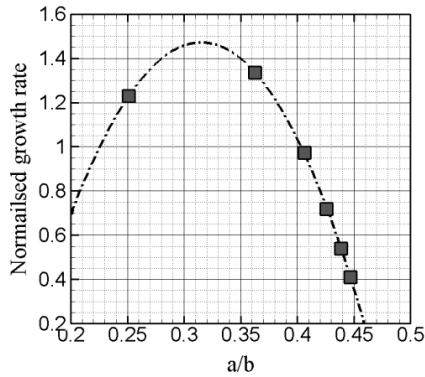


Figure 7: growth rate of peak instability mode for each separation case.

COUPLING OF VORTICES

Figure 8 shows the perturbation fields of the dominant instability modes for a range of a/b . The images are created by subtracting two slices of the vorticity field half a period out of phase. The blue and red zones in figure 8 are the same structure at different points in the stream tube.

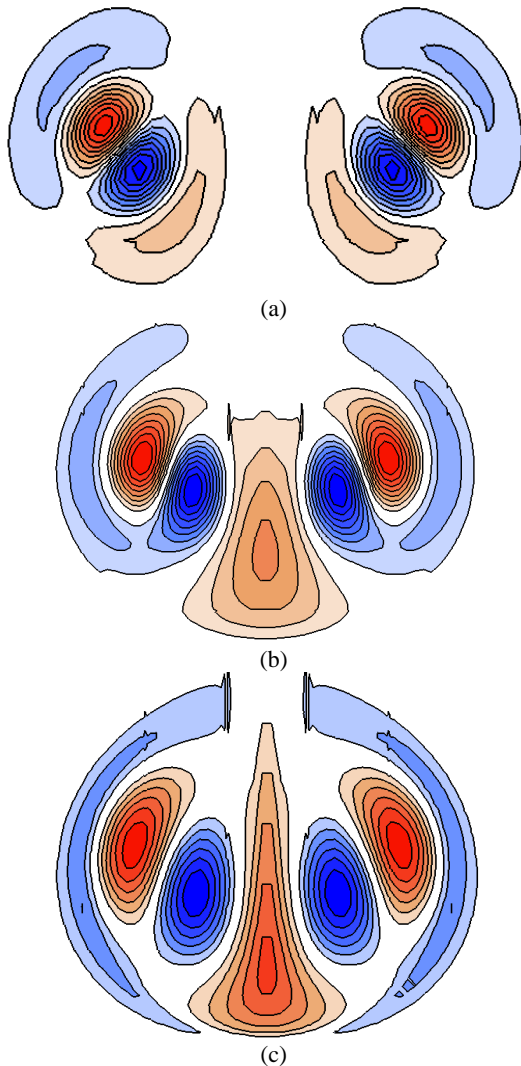


Figure 8: Contours of the vorticity fields for the principal mode corresponding to the $\lambda/a = 2.8$ peak in figure 6, a) $a/b=0.251$, b) $a/b=0.3625$, c) $a/b=0.4385$.

At large separation distances, as seen in figure 8a), the perturbation vorticity field in each vortex stream tube is comprised of two distinct regions. An inner region exists of high perturbation vorticity that sits within the characteristic core radii, and a less intense outer region that curls around in a crescent shape offset from the vortex core. These may be analyzed as a pair of co-rotating perturbation vortices formed in each stream tube of the perturbation field. Figure 9 shows a three dimensional representation of the perturbation field for $a/b=0.251$.

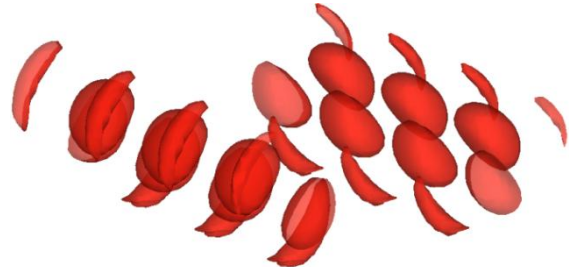


Figure 9: a 3D extrapolation of the perturbation vorticity field at relatively distant vortex spacing $a/b=0.251$. Vorticity of each iso-surface is $\omega_z=4.0$ Note the sinusoidal nature of the perturbation fields with the pairs of vortices seen in figure 8a).

As the two base vortices are brought closer together, the outer perturbation vortices from each stream tube undergo vortex merging, coupling the perturbation vortices. This region spikes up sharply along the centreline between the stream tubes. This occurs because the stream tubes are close enough for each of the outer co-rotating vortices to merge, forming a single perturbation vortex core. Leweke and Meunier (2005) demonstrated this in co-rotating pairs and is shown in figure 10. The correlation between the periodic nature of the convergence and the phase of the disturbance indicates a direct relationship between the precession rate of the co-rotating vortices and the disturbance frequency.

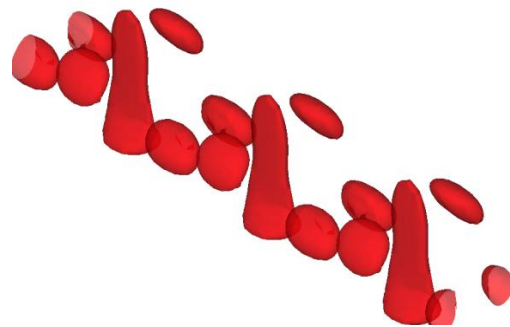


Figure 10: A 3D extrapolation of the perturbation vorticity field at vortex spacing $a/b=0.447$. Each iso-surface is $\omega_z=0.28$ Note the merged vortex structure in 3D which corresponds to the structure of 8b-c.

As the base vortex pair is brought still closer together, we see an increase in the relative strength of this perturbation vorticity region compared to the maximum perturbation vorticity in the vortex plane. This is shown in the progression of contours in figure 8 a-c. The relative increase in the strength of the coupled region with respect to the vortex core region amplifies the coupling effect.

THE COMPLETE THREE DIMENSIONAL FIELD

Figure 11 shows a three dimensional reconstruction of the complete flow field defined as the addition of the base

field to the perturbation field multiplied by an arbitrary value. It shows a periodic crossover of fluid between the each vortex in the pair. This is observed as small bulges emanating from the vortex stream tubes. These features are better developed in figure 11 a) where the vortices are closely spaced. These structures are evident at both close and distant separations, however at the distant separation a resolution 31 times greater is required for them to be seen.

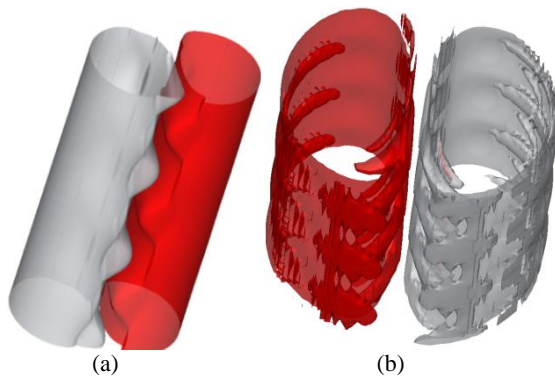


Figure 11: A 3D reconstruction of vortex iso-surfaces with fluid crossover regions shown. a) is the case $a/b=0.447$, b) is the case $a/b=0.251$.

Leweke and Williamson (1998) and Ryan and Sheard (2007) showed that growing deformations of the short-wave instabilities give rise to periodic cross-over of fluid between vortices. This creates an array of secondary vortices perpendicular to the primary pairs, which quickly lead to the breakdown of primary vortex circulation. In figure 8 we see the growth of the periodic fluid cross-over regions. These form as the coupled region of the perturbation field acts as a vortex, drawing fluid from each base vortex stream tube, which in turn allows fluid cross-over. This was previously only observed during the non-linear growth period. However this analysis shows that it is in fact due to the principal linear growth mode. We postulate that the growth of the fluid crossovers and eventual secondary vortex production are accelerated by the non-linear growth regime as well as by close proximity of the vortices. In either case this allows coupling of the perturbation vorticity field (shown in figure 8).

This study was limited in that it did not include turbulence modelling, or account for any axial flow. While an error of only 3.8% allows excellent qualitative analysis, 3D simulations with the addition of an axial velocity component, like that of a Batchelor vortex pair would further refine the analytical model and support the analysis conducted in this paper.

CONCLUSIONS

This investigation has considered the growth of short-wave elliptical instabilities in a Lamb-Oseen vortex pair subject to non-uniform strain fields at close vortex spacing, using DNS. Previous research has been conducted at large vortex spacing, where the mutually induced strain field that causes the elliptical deformation of vortex cores is typically uniform. This study investigated the instability growth over a range of wave-numbers as the vortex spacing is reduced.

A limit of minimum vortex spacing was found via a viscous diffusion method previously employed by Le Dizès and Verga (2002). A counter-rotating vortex pair with equal circulation magnitude may not exist closer than

a separation ratio of $a/b=0.5$. This indicates that the vortex pair exerts a mutual force on each vortex such that invariant streamlines may not overlap.

The perturbation analysis of the vortices was conducted by developing linear modes over a frozen base flow. It was found that as vortex spacing is reduced, growth rate of non-principal wave-numbers is enhanced relative to principal wave-numbers. The peak growth rate of the principal instability mode reduced as the vortices were brought closer together. At other wave-numbers, the growth rate increased relative to the peak, resulting in a broadening of the growth rate profile.

The perturbation field was shown to be composed of a pair of co-rotating vortices in each stream tube, which could merge at close vortex spacing to cause coupling of the vortex stream tubes in the fluid cross over region. These fluid cross over regions, which were shown to be products of a linear growth regime, were shown to exist at large separations but were greatly enhanced at close separations. The dissipation of vortex pairs is an important field of study for the aviation industry, in which enhanced vortex dissipation may lead to increased efficiency of air infrastructure. It should therefore be considered in future wing design.

REFERENCES

- LACAZE, L., RYAN, K. and LE DIZES, S. (2006) "Elliptic instability in a strained Batchelor vortex". *J. Fluid Mech.* **577**, 341-261
- LE DIZES, S. and LAPORTE, F. (2002) "theoretical predictions for the elliptical instability in a two-vortex flow." *J. Fluid Mech.* **471**, 169-201
- LE DIZES, S. and VERGA, A., (2002) "Viscous interactions of two co-rotating vortices before merging." *J. Fluid Mech.* **467**, 389-410
- SHEARD, G.J., FITZGERALD, M.J. and RYAN, K. (2009) "Cylinders with square cross section: Wake instabilities with incidence angle variation." *Journal of Fluid Mechanics* **630**, 43-69
- SHEARD, G. J., LEWEKE, T., THOMPSON, M.C., and HOURIGAN, K. (2007) "Flow around an impulsively arrested circular cylinder" *Physics of Fluids* **19**, 8
- SHEARD, G. J. and MEUNIER, P. (2005) "Elliptic instability of a co-rotating vortex pair" *J. Fluid Mech.* **533**, 125-159
- LEWEKE, T. and WILLIAMSON, C. H. K. (1998) "Cooperative elliptic instability in a vortex pair." *J. Fluid Mech.* **360**, 85-119
- PHILLIPS, F. (2004). *Mechanics of flight. Wiley and sons*
- RYAN, K. and SHEARD, G. J. (2007) "Non-linear growth of short-wave instabilities in a Batchelor vortex pair." *Proceedings of the 16th Australasian fluid mechanics conference, Gold Coast, Australia 2-7 December 2007.*
- SPALART, P. (1998) "Airplane trailing vortices." *Annu. Rev. Fluid Mech.* **30**, 107-138